

Fig. 4 *a*, Group of *Festuca* roots from field inoculum system showing infection point (EP) arising from a fascicle of hyphae (EM) in which numerous chlamydospores (arrowed) are developing ($\times 40$). *b*, Autoradiograph of this group showing accumulation of radioactivity at the entry point (EP), in vesicles (V) and arbuscules (A) along the infected root, in the mycelial fascicle (EM) and in the developing spores. Uninfected roots contain little or no labelled material ($\times 40$).

from which infection has spread. There is the further possibility that during the critical establishment phase the entire seedling may live for a period in partial heterotrophic dependence upon its neighbours. The extent of this dependence will be revealed in experiments now being conducted over a longer time period.

We thank Dr F. E. Sanders and Mr L. Reed for supplying spores of *G. caledonium*.

Received 29 July; accepted 1 November 1983.

1. Read, D. J., Koucheki, H. K. & Hodgson, J. H. *New Phytol.* **77**, 641-651 (1976).
2. Brownlee, C., Duddridge, J. A., Malibari, A. & Read, D. J. *Pl. Soil* **71**, 433-443 (1983).
3. Reid, C. P. P. & Woods, F. W. *Ecology* **50**, 178-187 (1969).
4. Hirrel, M. C. & Gerdemann, J. W. *New Phytol.* **83**, 731-738 (1979).
5. Heap, A. J. & Newman, E. I. *New Phytol.* **5**, 173-180 (1980).
6. Whittingham, J. & Read, D. J. *New Phytol.* **90**, 277-284 (1982).
7. Chiariello, N., Hickman, J. C. & Mooney, H. A. *Science* **217**, 941-943 (1982).
8. Ho, I. & Trappe, J. M. *Nature* **244**, 30-31 (1973).
9. Cox, G., Sanders, F. E., Tinker, P. B. & Wild, J. A. in *Endomycorrhizas* (eds Sanders, F. E., Mosse, B. & Tinker, P. B.) 297-312 (Academic, London, 1975).
10. Buwalda, J. G. & Goh, K. M. *Soil. Biol. Biochem.* **14**, 103-106 (1982).
11. Snellgrove, R. C., Splittstoesser, W. E., Stribley, D. P. & Tinker, P. B. *New Phytol.* **92**, 75-87 (1982).

X-ray diffraction evidence that actin is a 100 Å filament

E. H. Egelman

MRC Laboratory of Molecular Biology, Hills Road, Cambridge CB2 2QH, UK

R. Padrón

Laboratorio de Biofísica del Músculo, Centro de Biofísica y Bioquímica, Instituto Venezolano de Investigaciones Científicas, Caracas 1010A, Venezuela

The shape of the actin monomer has been determined by X-ray crystallography¹ and image analysis² to be a prolate ellipsoid consisting of two domains. A key structural question is how this monomer is assembled into the biologically important actin filament. Two completely different classes of models of F-actin have recently appeared. In one, the long axis of the monomer is oriented parallel to the filament axis^{1,2}, while in the other it is nearly perpendicular to that axis³⁻⁵. Fowler and Aebi⁶ have argued that a proper assessment of the diameter of the actin filament can distinguish between the correctness of these models, since the 'perpendicular' model is about 95 Å in diameter, while the 'parallel' model is about 75 Å in diameter. Using electron microscopy, they have determined the diameter to be between 70 and 80 Å, consistent with their model. Egelman and DeRosier³ also provided evidence from electron microscopy that the filament was about 95 Å, consistent with their perpendicular model. However, all specimens prepared for electron microscopy are susceptible to various artefacts induced by the preparation procedure. X-ray diffraction of specimens in solution allows one to examine objects in their native state. Data from X-ray diffraction of actin filaments in live muscle are presented here which show that a reasonable value for the diameter of F-actin is between 95 and 100 Å.

The strongest feature in the muscle X-ray pattern arising from the thin filament is the 59 Å layer line (the measured amplitude distribution is shown in Fig. 1A). Because of the different helical symmetries of actin and myosin in muscle, the 59 Å layer line arises only from the thin filament and is related to the distribution of density along the 59 Å left-handed one-start helix of the actin filament. Since the long-pitch strands of tropomyosin are nearly perpendicular to this short-pitch actin helix, tropomyosin will make almost no contribution at low resolution to the diffracted intensity along this layer line⁷. Therefore, by using the phases determined by electron microscopy of negatively stained filaments³ one can use the X-ray amplitudes to generate a projection of the actin density along this 59 Å helix. Computed transforms of negatively stained filaments showed that the phase was relatively flat across the single broad amplitude peak (considerations of phase continuity show that this must be the case for an object the approximate diameter of F-actin). The resulting helical projection is presented in a one dimensional form in Fig. 1B. The X-ray data used were of limited resolution (extending out to 0.020 Å⁻¹ from the meridian), but it is clear that any higher resolution data (out to 0.030 Å⁻¹) are weak and therefore could not dramatically change the distribution. A comparable helical projection (using the same resolution cutoff) obtained from the model of Egelman and DeRosier is also shown.

The model data match the X-ray data well, the only difference being that the observed data extend out further in radius than the model. The X-ray data shown are consistent with a filament having significant mass extending out to a 100 Å diameter, and are completely inconsistent with a 70-80 Å diameter filament. A comparable plot to Fig. 1B (data not shown) has been made using the recently published layer line intensities from a relaxed smooth muscle⁸. The intensity distribution shown by Tajima *et*

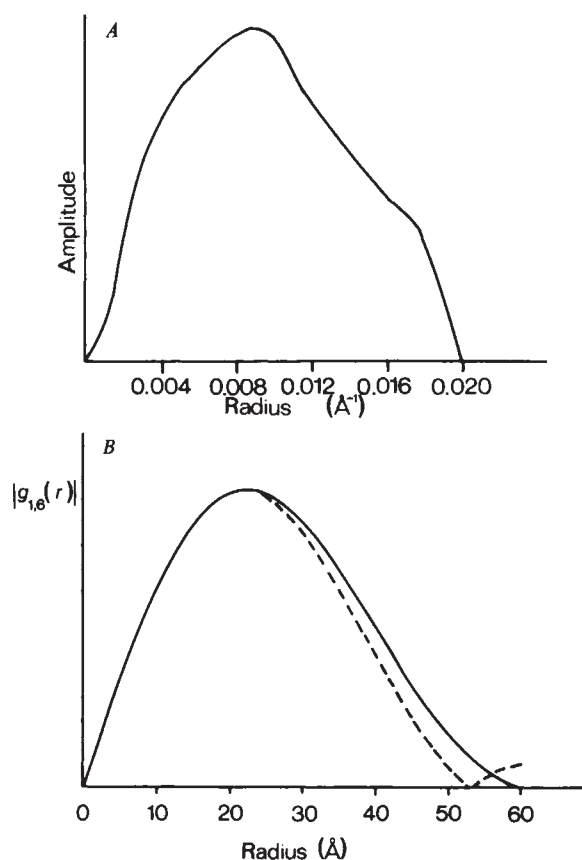


Fig. 1 *A*, The integrated intensity of the 59 Å layer line from the X-ray diffraction pattern of live relaxed frog sartorius muscle was measured, and a background was subtracted. The resulting amplitude distribution is shown. *B*, The function $g_{1,6}(r)$ (ref. 15) has then been computed using Fourier-Bessel inversion of the data shown in (*A*) (solid curve). A corresponding plot from the model of Egelman and DeRosier³ is also shown (dashed curve). This function is proportional to the modulation of F-actin density when the filament structure is projected along the 59 Å left-handed helix. Because the true radial density distribution of the filament (derived from the equator) has not been added in, this function is zero at the filament axis. The density distribution for the model extends beyond the 49 Å outer radius of the model because of the resolution cutoff which has been imposed to make the two plots comparable.

*al.*⁸ extends out to 0.024 \AA^{-1} on the 59 Å layer line, and the resulting helical projection agrees even better with the model. This suggests that the cutoff of our observed intensity at 0.020 \AA^{-1} is responsible for the difference which exists between the model helical projection and the X-ray derived projection.

A second line of X-ray evidence concerns the radius of gyration of the actin filament. This quantity is equal to the square root of the second moment of the average cross-sectional density distribution:

$$\left(\frac{\int r^2 \rho(r, \theta) r dr d\theta}{\int \rho(r, \theta) r dr d\theta} \right)^{1/2}$$

It has been measured to be $25 \pm 2 \text{ \AA}$ (ref. 9 and R. Mendelson, personal communication). A homogeneous cylinder (whose mean radial density distribution is given by a box function) will have a radius of gyration equal to $r_{\text{max}}/\sqrt{2}$, where r_{max} is the outer radius of the cylinder. Thus, the 25 Å value obtained implies that the radius of gyration of actin is the same as that of a homogeneous cylinder of maximum radius $\sqrt{2} \times 25 \text{ \AA}$, or 71 Å in diameter. This value was cited by Fowler and Aebi⁶ as being consistent with their 70–80 Å model. But we know, in fact, that actin is far from a solid cylinder. For one thing, it has a deep helical groove along the 59 Å helix which gives rise to the strong and broad peak along the 59 Å actin layer line. This

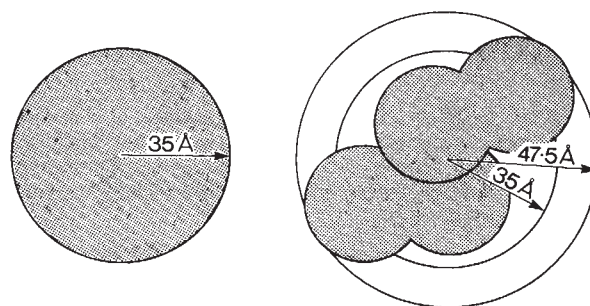


Fig. 2 The radial density distribution of two different models having the same radius of gyration (25 Å) as that experimentally determined for actin⁹ are compared. *A*, A homogeneous solid cylinder. *B*, Two actin subunits from the model of Egelman and DeRosier³, looking down the filament axis. The model uses two symmetrical spheres in the absence of any better information on which domain is the larger. The model is basically enclosed by a cylinder of 95 Å in diameter. The model's radius of gyration (25.4 Å) is equal to that of the solid cylinder shown in *A*.

is the most characteristic feature of both electron microscope transforms and X-ray patterns of actin. A consideration of how the actin subunit can be packed into a filament having such a groove suggests that proportionately more mass has been removed from the 'ideal' homogeneous cylinder at higher radius than at lower radius. This means that the mean radial density distribution will fall with radius. Therefore, the fact that actin has a radius of gyration equivalent to that of a homogeneous cylinder of 71 Å diameter is a strong argument that the maximum diameter of the actin filament is significantly greater than 71 Å. Figure 2 compares the radial density distribution of the 'perpendicular' actin model with that of a homogeneous cylinder having the same radius of gyration. The model of Egelman and DeRosier shown has a radius of gyration of 25.4 Å, in complete agreement with the measured value.

The third avenue of X-ray evidence arises from the early observations^{10,11} of the existence of a sixth layer line meridional reflection in the X-ray diffraction pattern of pure F-actin gels. Such a reflection is 'forbidden' by helical symmetry, and must arise from a perturbation of the axial distribution of mass in the actin filament. Lednev interpreted this feature in terms of subunits within the actin filament being in different states. Egelman and DeRosier¹² extended this, using evidence from Mg^{2+} paracrystals and the bending of stereocilia¹³ to show that the subunit within the actin filament possessed a variable tilt. They also argued that this feature, mediated by cross-bridging proteins in the stereocilia, arose only from inter-filament packing interactions in Mg^{2+} paracrystals. It is therefore important that Lednev first observed the existence of this reflection when the mean inter-filament spacing in a pure F-actin gel was slightly over 100 Å (ref. 10). At larger spacings this reflection disappeared. This was originally interpreted by Lednev to mean that this deformation of the filament structure occurred when filament surfaces were about 40 Å apart, assuming a 70 Å diameter filament (a traditional assumption). This observation is more consistent with a picture of direct contacts between 'fat' actin filaments inducing tilts of subunits within the filament. The original explanation, of filament conformation being mediated by long range forces, seems much less plausible.

Thus our determination of actin filament diameter using data from X-ray diffraction shows that the actin filament must have a diameter of about 100 Å, and that the perpendicular arrangement of subunits in the filament is required to account for this large outer diameter. Further, this orientation of the monomer is supported by image analysis of isolated actin filaments³, S-1 decorated actin⁴, and single-layered paracrystals of thin filaments⁵. The most likely origin of the parallel model of Smith *et al.*² remains the superposition problem associated with multiple layer paracrystals¹⁴.

We thank Dr H. E. Huxley for support and Dr L. Amos for helpful discussions. E.H.E. is a Fellow of the Jane Coffin Childs

Memorial Fund for Medical Research. This investigation has been aided by a grant from the Jane Coffin Childs Memorial Fund for Medical Research.

Note added in proof: The radius of gyration of F-actin has recently been remeasured and found to be $25.7 \pm 0.5 \text{ \AA}$ (P. Matsudaira, J. Bordas and M. Koch, personal communication). This is in agreement with the cited value⁹, but with a significantly smaller error.

Received 4 August; accepted 19 October 1983.

1. Suck, D., Kabsch, W. & Mannherz, H. G. *Proc. natn. Acad. Sci. U.S.A.* **78**, 4319–4323 (1981).
2. Smith, P. R., Fowler, W. E., Pollard, T. D. & Aebi, U. *J. molec. Biol.* **167**, 641–660 (1983).
3. Egelman, E. H. & DeRosier, D. J. *J. molec. Biol.* **116**, 623–629 (1983).
4. Taylor, K. A. & Amos, L. A. in *Actin: Its Structure and Function in Muscle and non-Muscle Cells* (eds dos Remedios, C. & Barden, J.) 25–26 (Academic, Sydney, 1983).
5. O'Brien, E. J., Couch, J., Johnson, G. R. P. & Morris, E. P. in *Actin: Its Structure and Function in Muscle and non-Muscle Cells* (eds dos Remedios, C. & Barden, J.) (Academic, Sydney, 1983).
6. Fowler, W. E. & Aebi, U. *J. Cell Biol.* **97**, 264–269 (1983).
7. Parry, D. A. D. & Squire, J. M. *J. molec. Biol.* **75**, 33–55 (1973).
8. Tajima, Y., Kamiya, K. & Seto, T. *Biophys. J.* **43**, 335–343 (1983).
9. Hartt, J. & Mendelson, R. *Fedn Proc.* **39**, 1728 (1980).
10. Lednev, V. in *Structural Basis and Regulation of Biological Movement* [Russian] (Nauka, Moscow, 1980).
11. Hanson, J., Lednev, V., O'Brien, E. J. & Bennett, P. M., *Cold Spring Harb. Symp. quant. Biol.* **37**, 311–318 (1972).
12. Egelman, E. H. & DeRosier, D. J. in *Actin: Its Structure and Function in Muscle and non-Muscle Cells* (eds dos Remedios, C. & Barden, J.) 17–24 (Academic, Sydney, 1983).
13. Tilney, L. G., Egelman, E. H., DeRosier, D. J. & Sänders, J. C. *J. Cell Biol.* **96**, 822–834 (1983).
14. Egelman, E. H., Frances, N. & DeRosier, D. J. *J. molec. Biol.* **116**, 605–622 (1983).
15. Klug, A., Crick, F. H. C. & Wyckoff, H. W. *Acta crystallogr. A* **11**, 199–213 (1958).

Direct observation of motion of single F-actin filaments in the presence of myosin

Toshio Yanagida, Michiyuki Nakase, Katsumi Nishiyama & Fumio Oosawa

Department of Biophysical Engineering, Faculty of Engineering Science, Osaka University, Toyonaka, Osaka, Japan

Actin is found in almost all kinds of non-muscle cells where it is thought to have an important role in cell motility. A proper understanding of that role will only be possible when reliable *in vitro* systems are available for investigating the interaction of cellular actin and myosin. A start has been made on several systems^{1–4}, most recently by Sheetz and Spudich who demonstrated unidirectional movement of HMM-coated beads along F-actin cables on arrays of chloroplasts exposed by dissection of a *Nitella* cell⁵. As an alternative approach, we report here the direct observation by fluorescence microscopy of the movements of single F-actin filaments interacting with soluble myosin fragments energized by Mg^{2+} -ATP.

Nagashima and Asakura reported that single filaments of F-actin decorated with heavy meromyosin (HMM) or S-1 are directly visible under an optical microscope with dark-field illumination, although the filaments without HMM or S-1 decoration are not visible⁶. Recently, S. Asakura (personal communication) found that single filaments of F-actin, without HMM or S-1 decoration, are made visible under a fluorescence microscope by labelling with fluorescein isothiocyanate. Using the fluorescent dye, phalloidin-rhodamine, we could clearly and continuously observe the movement of single filaments of F-actin or F-actin-tropomyosin (TM)-troponin (TN) complex for more than 5 min without photobleaching. Phalloidin-rhodamine is most convenient for the present purpose, because it is specifically bound to F-actin without any influence on physiological functions of F-actin^{7,8} and its fluorescence intensity is enhanced 4.2-fold by the binding.

When G-actin is polymerized in the presence of phalloidin-rhodamine, many filaments become visible under a fluorescence microscope. Figure 1 shows micrographs of phalloidin-

Table 1 Flexural rigidity (ϵ) of F-actin and F-actin-TM-TN complexes

Sample	Medium	λ (μm^{-1})	ϵ (10^{-17} dyn cm ²)
FA	+Ca	0.032	6.5
FA+HMM	+Ca	0.042	4.9
	+Ca+ATP	0.059*	3.5*
	–Ca	0.028	7.4
FA+TM+TN	+Ca	0.040	5.2
	–Ca	0.025	8.3
	+Ca	0.045	4.6
FA+TM+TN+HMM	–Ca+ATP	0.027	7.7
	+Ca+ATP	0.053*	3.9*
	–Ca	0.033	6.4
	+Ca	0.033	6.4

The concentration of HMM was 5 mg HMM ml⁻¹. +Ca, rigor buffer +0.2 mM CaCl₂; –Ca, rigor buffer +1 mM EGTA; +Ca+ATP, activating buffer; –Ca+ATP, relaxing buffer. The flexural rigidity, ϵ , was determined by measuring the end-to-end distance, R . About 50 values of R were measured for each filament in a 2–10-s period and the mean square end-to-end distance, $\langle R^2 \rangle$, was related to a parameter of flexibility, λ , by the equation $\langle R^2 \rangle = [2\lambda L - 1 + \exp(-2\lambda L)]/2\lambda^2$ (ref. 16). The most probable values of λ were obtained from a least-square fit to the plots of L versus $\sqrt{\langle R^2 \rangle}$ of more than 10 different filaments 5–10 μm in contour length, L . The flexural rigidity, ϵ , was calculated from the value of λ by the equation $\epsilon = kT/2\lambda$ (ref. 17). FA-PM, F-actin cross-linked by *p*-phenylene-*N,N'*-bis(maleimide) by the method of Knight and Offer¹⁴.

* In the activating buffer, the motion is not a thermal one, but the apparent values of λ and ϵ determined by the above procedure are shown for convenience to compare the extent of bending (see text).

rhodamine-labelled F-actin and F-actin-TM-TN complex in various conditions. All fluorescent filaments have the same brightness and the brightness is uniform along the filament. The number of filaments visible in the field of microscope agrees with the number expected from the concentration of F-actin. The visible filaments are not bundles of F-actin but single filaments of F-actin.

The thermal bending motion of the filaments is observable under the microscope. Table 1 gives the flexural rigidity of F-actin and F-actin-TM-TN complex estimated by the statistical analysis of the end-to-end distance of a number of filaments. The values of the flexural rigidity are in good agreement with those of unlabelled F-actin and F-actin-TM-TN measured by different methods^{6,9–11}. This indicates that the binding of phalloidin does not affect the dynamic property of F-actin although it stabilizes F-actin against depolymerization at low ionic strength or high concentration of KI¹². The binding of Ca²⁺ decreased the rigidity of the complex and the binding of HMM further decreased the rigidity in the presence of Ca²⁺.

When both HMM and Mg^{2+} -ATP are added to the F-actin-TM-TN complex in the presence of Ca²⁺, the bending motion of long filaments becomes faster and larger in amplitude, and the tumbling motion of shorter filaments becomes conspicuous. During such motions, long filaments are often broken into fragments of up to a few micrometres (Fig. 1d). Figure 2 shows sequences of micrographs taken to compare the bending motion of the F-actin-TM-TN filaments in a solution containing HMM and Mg^{2+} -ATP, in the absence (Fig. 2a) and presence (Fig. 2b) of Ca²⁺. The filaments in Fig. 2a and b have same length, 10 μm . In the absence of Ca²⁺ (Fig. 2a), the bending motion of the first order mode has an apparent period of 3–6 s, and that of the second order mode has a period of about 0.3 s. Previously, by using dynamic light scattering, the relaxation time of the bending motion of F-actin of 2.5 μm in length was determined to be about 10 ms⁹. The above value, 3–6 s, for the filaments of 10 μm length is reasonable because the relaxation time, τ_n , of the bending motion is proportional to the fourth power of the length, as given by

$$\tau_n = \pi^{-4} (n + (1/2))^{-4} \zeta L^4 \epsilon^{-1} \quad (1)$$

where n is the mode number, L the contour length of the filament, ζ the frictional constant for a structural unit and ϵ the flexural rigidity⁹.

In the presence of Ca²⁺ (Fig. 2b), the apparent period of the bending motion of the first mode decreased to 1–3 s. If the bending is due to thermal brownian motion, the flexural rigidity in the presence of Ca²⁺ must be about twice as large as that in its absence, according to equation (1). However, as found in